

# A Simple Relationship for High Efficiency–Gradient Uniformity Tradeoff in Multilayer Asymmetric Gradient Coils for Magnetic Resonance Imaging

H. Sánchez, F. Liu, A. Trakic, and S. Crozier

School of Information Technology and Electrical Engineering, University of Queensland, St. Lucia, Brisbane Ald 4072, Australia

**High-quality gradient coils are pivotal to advances in magnetic resonance imaging (MRI). We have studied the influence of coil dimensions and target requirements in multilayer, asymmetric, transverse gradient coils. We developed a simple linear function that defines the optimal coil length to produce a maximum figure of merit given an imaging region size and location, coil radius, and gradient nonuniformity. Our method, based on the linear function, yields high-quality solutions. The method introduces two torque/force minimization strategies in order to obtain asymmetric transverse gradient coils that balance minimum torque with a maximum figure of merit. High-performance head, asymmetric gradient coils with simple current patterns and minimum torque can be tailored to a specific magnet design, as we illustrate.**

**Index Terms**—Gradient coil design, magnetic resonance imaging (MRI), peripheral nervous stimulation, target field approach.

## I. INTRODUCTION

**N**EW architectures for magnetic resonance imaging (MRI) systems require an integrated design that takes into account the complex inter-relationships between the electrical, mechanical, and magnetic field constraints in each subsystem (e.g., magnet, gradient, shim coils). The main magnet must produce a very homogenous and stable magnetic field in a relatively large diameter spherical volume (DSV) of 40 to 50 cm. It becomes more difficult to satisfy all the required constraints as the length of the magnet is reduced [1], [2]. One of the first trials to study the relationship between cost and magnet length was presented by H. Xu *et al.* [3]. In this work, a simple linear relationship for the main magnet length that produces minimum cost as function of DSV and coil radius was derived.

The reduction of the magnet length impacts directly on the gradient coil constraints and coil performance. In the design of short gradient coils, it is difficult to control the residual eddy currents in the cryostat, as more current is necessary to produce the same gradient strength; the winding patterns and the cooling system become more complex.

Gradient coil performance can be measured with a figure of merit given by  $M = (\eta^2 \rho_1^5)/L$ , where  $L$ : inductance (H),  $\eta$ : efficiency (in T/m/A),  $\rho_1$ : coil radius (m). A high-performance gradient coil is characterized by a high efficiency  $\eta$  and low inductance  $L$ . The efficiency  $\eta$  is defined as the ratio between the gradient strength  $G_0$  produced by the coil at the center of DSV and the operating current  $I$ ;  $\eta$  is proportional to  $N/\rho_1^2$ ; where  $N$  is the number of turns. The inductance is proportional to  $N^2 \cdot \rho_1$ . In order to compare the performance of gradient coils with different radii and ampere-turns, the efficiency and the coil radius are elevated to powers of two and five, respectively.

The figure of merit  $M$  is strongly affected when the coil length is reduced. In order to obtain a tradeoff between the coil performance and reduction in coil length, a linear function for the shortest gradient coil length to produce high-performance symmetric transverse gradient coils has been presented for fixed target magnetic field uniformity [4].

Along with the desired high performance  $M$ , the gradient coil must generate a highly linear magnetic field in the DSV. Gradient coils can generate high spatial gradient field uniformity in detriment to the figure of merit or one can obtain gradient coils with high performance  $M$  by relaxing the target spatial magnetic field quality. It is not clear, however, how the relaxed target field uniformity is related to the figure of merit for a given coil length, coil diameter, and DSV.

The purpose of this work is to study how this relaxation is related to the coil geometry to obtain an optimal tradeoff between coil performance and the target spatial gradient uniformity. A simple linear function that defines the optimal coil length to produce a maximum figure of merit given DSV size and location, coil radius, and a specified nonuniformity is obtained.

In this work, we also present two ways to reduce the undesired net torque produced due to the asymmetric nature of Lorentz force generated by the interaction between the static main magnetic field and the gradient coil current. By studying the effect of torque minimization on gradient coil performance, we show that a reduction of up to 80% in net torque decreases the figure of merit by only 5% from its maximum value. Simple current patterns for minimum torque, high-performance head asymmetric transverse gradient coils are obtained combining the magnetic field profile of a specified main magnet over the gradient coil with a specific axial position of the gradient coil's linear region.

## II. MATERIALS AND METHODS

In order to obtain a relationship between the figure of merit, target gradient uniformity, coil radius, axial coil length, and the DSV, it is necessary to define a design method that permits a

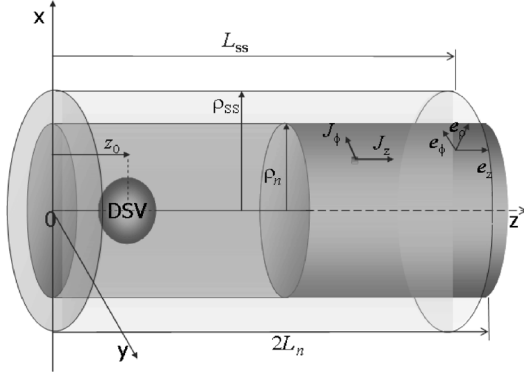


Fig. 1. Diagram illustrating the cylindrical surface of radius  $\rho_n$  and length  $2L_n$  where the current density  $\mathbf{J}$  flows. For simplicity only the surface  $n$  has been represented. The cylindrical surface of radius  $\rho_{SS}$  and axial length  $L_{SS}$  represents the surface at which the axial component of the magnetic field is constrained to a minimum value. The spherical region located at the axial position  $z_0$  represents the gradient coil DSV.

controlled relaxation of the target gradient uniformity. Through this relaxation factor we can control the expected tradeoff between the coil performance and the generated spatial gradient field uniformity. Also, a simple and computationally inexpensive method (minimum memory and calculation overhead) to produce several solutions in a relatively short time is desirable. We illustrate the method with an example multilayer, asymmetric transverse gradient coil design.

#### A. Magnetic Field, Energy and Force/Torque Calculation for Multilayer Asymmetric Gradient Coils

In the present method, we assume  $N$  layers of current density  $\mathbf{J}(\rho, \phi, z)$  flowing in concentric cylindrical surfaces of radii  $\rho_n$ . The current density distribution is confined in the interval ( $Z_i \leq z \leq Z_f$ ). The variables  $Z_i = 0$  and  $Z_f = 2L_n$  define the initial and the final axial limits of  $\mathbf{J}$  for asymmetric gradient coils, where  $2L_n$  is the coil length for layer  $n$  (see Fig. 1). It is assumed that the radial thickness of the surface is much smaller than the cylindrical radius  $\rho_1$ . Thus, the vector current density  $\mathbf{J}(\rho, \phi, z)$  is described in terms of the azimuthal and axial components only. We use the Carlson's approach to generate coils of finite length [5]. The azimuthal component of the current density is expressed as a sum of orthonormal functions multiplied by the amplitudes  $a_{nq}$  that appear in the following expression [6]:

$$J_\phi(\rho, \phi, z) = \sum_{n=1}^N \sum_{q=1}^Q h_{nq}^\phi(\rho, \phi, z) a_{nq} \quad (1)$$

where

$$h_{nq}^\phi(\rho, \phi, z) = \delta(\rho - \rho_n) H(z) H(2L_n - z) \times \left\{ \begin{array}{l} \sin(k_q z) \\ \cos(k_q z) \cos(\phi) \end{array} \right\}. \quad (2)$$

$k_q = \pi q / L_n$ ,  $a_{nq}$  is the amplitude of each axial oscillation mode of  $J_\phi$ ,  $H(x)$  is the Heaviside function, which takes a value of 0 for  $x < 0$  and 1 for  $x > 0$ ,  $Q$  is the number of axial modes of the current density and  $\delta(\rho - \rho_n) = 1$  when  $\rho = \rho_n$ , otherwise

$\delta(\rho - \rho_n) = 0$ . The upper terms in the brackets correspond to the longitudinal gradient coil and the lower to the transverse gradient coil.

Due to the zero divergence of the continuity condition, the azimuthal and the axial components of  $\mathbf{J}(\rho, \phi, z)$  are related and the coil design is completely described in terms of  $J_\phi(\phi, z)$ .

The axial component of the magnetic field  $B_z$  produced by a small superficial current element area  $dS' = \rho_n d\phi' dz'$  of current density  $\mathbf{J}(\rho_n, \phi', z')$  at the observation point  $t(\rho, \phi, z)$  located in the DSV is the sum over all  $q$  axial oscillation modes of the current density corresponding to each layer  $n$  of axial length  $2L_n$  and radius  $\rho_n$ . Applying Biot-Savart's law,  $B_z$  is calculated as

$$B_z(\rho, \phi, z) = \sum_{n=1}^N \sum_{q=1}^Q B_{z_{qn}} a_{nq} \quad (3)$$

where

$$B_{z_{qn}} = \frac{\mu_0}{4\pi} \times \int_0^{2\pi} \int_{Z_i}^{Z_f} \frac{(\rho \cos(\phi - \phi') - \rho_n) h_{nq}^\phi(\rho_n, \phi', z') dS'}{R^3} \quad (4)$$

and  $R = \sqrt{\rho^2 + \rho_n^2 - 2\rho_n\rho \cos(\phi - \phi') + (z - z')^2}$  is the distance between current source of area  $dS'$  and the observation point  $t$ .

The methodological approach used in this work to calculate the axial magnetic field component by Biot-Savart's law can be extended to an arbitrary geometrical surface taking into account the selection of an adequate current density function according to the gradient design problem.

In order to implement a general method for gradient coil designs of arbitrary geometry, the current surface is divided into a small mesh of elemental areas assuming a basis stream function multiplied by unknown amplitudes [7].

The rate of change of  $B_z(\rho, \phi, z)$  in respect to the Cartesian  $x$ -coordinate ( $G_x = \partial B_z / \partial x$ ) for the transverse gradient coil is used to calculate the gradient field contribution of all axial modes of the current density  $\mathbf{J}$  at the target point  $t$  located in the DSV. The expression can be derived from (3) and

$$G_x(\rho, \phi, z) = \sum_{n=1}^N \sum_{q=1}^Q G_{x_{qn}} a_{nq} \quad (5)$$

where

$$G_{x_{qn}} = -\frac{\mu_0}{4\pi} \int_0^{2\pi} \int_{Z_i}^{Z_f} h_{nq}^\phi(\rho_n, \phi', z') \times \left[ \frac{\cos(\phi')}{R^3} - \frac{3(\rho \cos(\phi - \phi') - \rho_n)(\rho \cos(\phi) - \rho_n \cos(\phi'))}{R^5} \right] dS'. \quad (6)$$

For longitudinal gradient coil  $G_z = \partial B_z / \partial z$  is written as

$$G_z(\rho, \phi, z) = \sum_{n=1}^N \sum_{q=1}^Q G_{z_{qn}} a_{nq} \quad (7)$$

where

$$G_{z_{qn}} = -\frac{\mu_0}{4\pi} \times \int_0^{2\pi} \int_{Z_i}^{Z_f} h_{nq}^\phi(\rho_n, \phi', z') \times \left[ \frac{3(\rho \cos(\phi - \phi') - \rho_n)(z - z') dS'}{R^5} \right]. \quad (8)$$

In our approach, (3) is used to calculate the magnetic field contribution at the target surface of radius  $\rho_{SS}$  and axial length  $L_{SS}$  (see Fig. 1), where the magnetic field is constrained to a minimum value.

The magnetic field gradient condition at a point  $t$  located within the DSV is expressed as relaxed linear constraint as follows:

$$|G_{x(z)_t} - G_0| \leq \varepsilon G_0; \quad t = 1 \dots T \quad (9)$$

where  $T$  is the number of target points in the DSV;  $G_0$  measured in (T/m), is the target gradient strength specified at the target point  $t$ ,  $\varepsilon$  is the relaxation factor or the introduced nonuniformity error. The  $\varepsilon$  parameter allows control over the desired target gradient uniformity and at the same time relaxes the boundary conditions in the DSV. When high-frequency spatial changes in the current density are produced due to stringent constraints included in the design problem, the parameter  $\varepsilon$  contributes to the minimization of these undesired spatial oscillations. The factor  $\varepsilon$  increases the solution space and hence improved configurations with more balanced performance can be obtained. If the relaxation factor is  $\varepsilon = 0.025$  (i.e., 2.5%), then the resulting target uniformity peak to peak is equal to 5% of relative deviation from  $G_0$ .

The stored magnetic energy is calculated in Fourier space rather than the real space. For the transverse gradient coils, we define the stored magnetic energy as

$$E = \sum_{n=1}^N \sum_{q=1}^Q \sum_{n'=1}^N \sum_{q'=1}^Q E_{nqn'q'} a_{nq} a_{n'q'}. \quad (10)$$

The matrix  $E_{nqn'q'}$  contains the self and all the mutual magnetic energy interactions among all axial modes of  $\mathbf{J}$  flowing in the cylindrical surfaces. Using (10), the magnetic energy can be efficiently evaluated with a small computational burden.

In order to calculate the force/torque acting on the superficial continuous current density due to an external main magnetic field, it is assumed that the surface is divided into  $U$  small elemental areas  $A$  whereby the current density  $\mathbf{J}$  is considered constant throughout the element. We assume as an external magnetic field the map profile of  $\mathbf{B}^{\text{main}}$  produced by the main magnet and the magnetic field  $\mathbf{B}^S$  generated by all the elemental areas  $A_u$  of the  $N$  surfaces. For asymmetric transverse gradient coil case, the component of the force that significantly contributes [8]–[13] to the vector amplitude is written as

$$F_{i_x} = \sum_{n=1}^N \sum_{q=1}^Q a_{nq} F_{x_{nq}} \quad (11)$$

where

$$F_{x_{nq}} = \sum_{u=1}^U F_{nq_u}^p \cdot \cos(\phi_u) - F_{nq_u}^\phi \sin(\phi_u) \quad (12)$$

$$F_{nq_u}^p = (h_{nq}^\phi(\mathbf{r}'_u) (B_{\mathbf{e}_z}^{\text{main}}(\mathbf{r}'_u) + B_{\mathbf{e}_z}^S(\mathbf{r}'_u))) A_u \quad (13)$$

and

$$F_{nq_u}^\phi = (f_{nq}^z(\mathbf{r}'_u) (B_{\mathbf{e}_\rho}^{\text{main}}(\mathbf{r}'_u) + B_{\mathbf{e}_\rho}^S(\mathbf{r}'_u))) A_u. \quad (14)$$

$f_{nq}^z(\mathbf{r}'_u)$  can be found applying the zero divergence of the continuity condition and  $\mathbf{r}'_u \equiv (\rho_n, \phi'_u, z'_u)$  is the vector that points the location of the elemental area  $A_u$ . Note that the azimuthal (1) and the axial components of the current density  $\mathbf{J}$  for the asymmetric transverse gradient coils case have been included in (11).

Using the expression  $\mathbf{T} = \mathbf{r} \times \mathbf{F}$ , we deduce the acting torque over the superficial elemental area  $A_u$ . The component that significantly contributes [8]–[13] to the vector amplitude can be written as

$$T_{j_y} = \sum_{n=1}^N \sum_{q=1}^Q a_{nq} T_{y_{nq}} \quad (15)$$

where

$$T_{y_{nq}} = \sum_{u=1}^U (F_{nq_u}^\phi z_u \sin(\phi_u) - (F_{nq_u}^z \rho_n - F_{nq_u}^p z_u) \cos(\phi_u)) \quad (16)$$

and

$$F_{nq}^z = - (h_{nq}^\phi(\mathbf{r}'_u) (B_{\mathbf{e}_\rho}^{\text{main}}(\mathbf{r}'_u) + B_{\mathbf{e}_\rho}^S(\mathbf{r}'_u))) A_u. \quad (17)$$

Some authors assume that the external magnetic field  $B_{\mathbf{e}_z}^{\text{main}}(\mathbf{r}'_u)$  is perfectly homogenous and  $B_{\mathbf{e}_\rho}^{\text{main}}(\mathbf{r}'_u) = 0$ ,  $B_{\mathbf{e}_\phi}^S(\mathbf{r}'_u) = 0$ ,  $B_{\mathbf{e}_z}^S(\mathbf{r}'_u) = 0$ ,  $B_{\mathbf{e}_\rho}^S(\mathbf{r}'_u) = 0$ . This assumption introduces considerable errors in the force/torque calculations when an asymmetric gradient coil is installed in short or asymmetric magnets. In our work, we consider the axial and the radial components of the magnetic field generated by the main magnet. In the net torque/force calculation, we take into account all such components.

### B. Problem Statement for Asymmetric Multilayer Transverse Gradient Coil

The magnetic field, magnetic field gradient, and torque/force expressions presented in this work are linear functions of the current density  $\mathbf{J}$ . This means that the magnetic field and torque/force conditions can be included as linear constraints in an optimization algorithm. Regarding to the defined figure of merit  $M$ , a high-performance gradient coil must produce low magnetic energy and high efficiency. It is possible to define the optimization problem as the minimization of  $E/G_0^2 \rho_1^5$  under linear constraints. Due to the quadratic relationship between the stored magnetic energy  $E$  and the amplitude  $a_{nq}$ , the multilayer

asymmetric transverse gradient coil design can be stated as a quadratic programming optimization problem as follows:

$$\begin{aligned}
\text{Min} : & \frac{1}{G_0^2 \rho_1^5} \sum_{n=1}^N \sum_{q=1}^Q \sum_{n'=1}^N \sum_{q'=1}^Q E_{nqn'q'} a_{nq} a_{n'q'} \\
\text{Subject} : & \\
& \sum_{n=1}^N \sum_{q=1}^Q G_{x_{qnt}} a_{nq} \leq G_0(1 + \varepsilon) \quad t = 1, \dots, T, \\
& - \sum_{n=1}^N \sum_{q=1}^Q G_{x_{qnt}} a_{nq} \leq -G_0(1 - \varepsilon) \quad t = 1, \dots, T, \\
& \left| \sum_{n=1}^N \sum_{q=1}^Q (B_{z_{x_{qnt}}} a_{nq}) \right| \leq B_{z_t}^{\text{Shield}} \quad t = T + 1, \dots, T + P \\
& \left| \sum_{n=1}^N \sum_{q=1}^Q (T_{y_{nq}} a_{nq}) \right| \leq T_{y0} \\
& \left| \sum_{n=1}^N \sum_{q=1}^Q (F_{x_{nq}} a_{nq}) \right| \leq F_{x0}. \tag{18}
\end{aligned}$$

In order to solve the problem stated in (18), we have employed the function *quadprog* provided in the MATLAB optimization toolbox. The algorithm searches for the minimum current density amplitudes  $a_{nq}$  that maximizes the coil performance and at the same time fulfill the relaxed linear gradient field conditions under constrained values of torque ( $T_{y0}$ )/force ( $F_{x0}$ ) and the axial component of magnetic field  $B_{z_t}^{\text{Shield}}$  specified at  $P$  points located at the cylindrical surface of radius  $\rho_{SS}$  and axial length  $L_{SS}$  (see Fig. 1). Instead of minimizing magnetic fields at the first eddy current source, one can control residual eddy current (REC) effects in the DSV [14]. To achieve this, the stored magnetic energy contribution generated by the REC induced in the surrounding conducting materials, should be also included in (10).

Although the optimization problem stated in (18) has been written in this work for multilayer asymmetric transverse gradient coil designs supported by cylindrical surfaces, it can be extended to gradient coil design with arbitrary surfaces using any well-defined stream function. In (18), one can include the remaining components of torque and force or all the parameters that have a linear relationship with the unknown current amplitude. These parameters are then to be constrained to certain values. Note in (18) that instead of balancing the constraints through weighting factors, a nonuniformity error  $\varepsilon$  is introduced in order to balance the figure of merit  $M$  with competing gradient uniformity, shielding, and minimal force/torque requirements. Moreover, the linear inequality constraints are not constrained to null values and this helps to achieve practical and high-performance solutions.

From the optimization problem stated in (18), it is also clear that magnetic energy, force/torque, and magnetic field can be computed on different CPUs (parallel network) in order to speed up the computation, if required.

### C. Figure of Merit Tradeoff

The figure of merit  $M$  is used as the measure of performance, due to its independence of the ampere-turns and coil radius.

Thus, for a fixed target gradient uniformity and DSV size, if the coil dimensions are scaled, the figure of merit will remain constant [4].

Thousands of multilayer asymmetric transverse gradient coils were calculated for different  $2L_1/\text{DSV}$  and fixed values for the number of current density layers ( $N = 1, 2, 3, 4$ ), target nonuniformity error  $\varepsilon$ , axial offset position of DSV ( $z_0$ ), and  $D_1/\text{DSV}$ .  $D_1$  is the coil diameter of the first layer ( $D_1 = 2\rho_1$ ). In order to reduce the number of parameters to be varied, we have normalized the axial coil length  $2L_1$  and the diameter  $D_1$  with respect to the coil DSV. In the case of  $N = 1$ , the shielding constraint was not included.

In order to study the influence of the relaxing factor  $\varepsilon$  over the figure of merit, we have varied  $\varepsilon$  from a relatively high target gradient uniformity (with  $\varepsilon = 0.01$ ) to a relatively low target gradient uniformity (with  $\varepsilon = 0.1$ ). The  $2L_1/\text{DSV}$  and  $D_1/\text{DSV}$  ratios were varied between 2–5.5 and 1.4–2.5, respectively, in order to produce practical solutions. The  $N$  radial cylindrical surfaces of current were equally spaced between the coil radius  $\rho_1$  and  $1.24 \cdot \rho_1$ . The axial lengths of the  $N$  cylindrical surfaces of current were equally distributed between  $2L_1$  and  $1.24 \cdot 2L_1$  for the  $N$  cylindrical surfaces. With this distribution, the current layer  $n = 1$  has the smaller radius and axial length and the current layer  $n = N$  has the larger radius and axial length to assure an effective active shielding. The axial component of the magnetic field was constrained to a minimum value in the range  $(-B_{z_t}^{\text{Shield}}, B_{z_t}^{\text{Shield}})$  on the surface of radius  $\rho_{SS} = 1.5 \cdot \rho_1$  and axial length  $L_{SS} = 2L_1$ .

In an asymmetric gradient coil design, it is desirable to locate the DSV region close to the coil edge [9] for patient comfort and imaging purposes. In this work, we have studied the influence of the DSV position  $z_0$  over the coil performance. For this purpose, three relatively large DSV axial offset values were considered  $z_0 = 2(L_1/4.1, L_1/3.6, L_1/3.1)$ .

In this study, the number of magnetic field linear constraints was equal to the number of axial modes of  $\mathbf{J}$ . At this stage, the force/torque constraints were not included in the analysis process.

For the selected relaxing factor  $\varepsilon$  and DSV axial position  $z_0$  values, we chose the coordinate pair  $(D_1/\text{DSV}, 2L_1/\text{DSV})$  for which the coil performance  $M$  is maximum. Then, using a curve-fitting algorithm, an optimal coil length function that produces maximal figure of merit given the coil diameter ( $D_1$ ) and DSV for fixed relaxing factor  $\varepsilon$  and axial DSV position  $z_0$  values, is obtained.

## III. RESULTS AND DISCUSSIONS

Applying our method for the range of coil parameters mentioned in the Section II-C, it was observed that for a number of layers  $N > 1$ , when the  $N$  value is increased for fixed  $2L_1/\text{DSV}$ ,  $D_1/\text{DSV}$  ratios, relaxing factor  $\varepsilon$  and axial DSV position  $z_0$ , the coil performance  $M$  decreases. This is due to the rate of change of coil inductance with respect to the number of layers  $N$  being larger than the rate of change of coil efficiency with respect to  $N$ . This effect is critical for coils with small axial lengths  $2L_1/\text{DSV} \leq 1$ . However, for our case ( $2L_1/\text{DSV} \geq 2$ ) where the axial coil length  $2L_1$  is twice the DSV, we realize that the change of figure of merit  $M$  with the total number of layers  $N$  can be assumed to be constant. Taking this into account, the

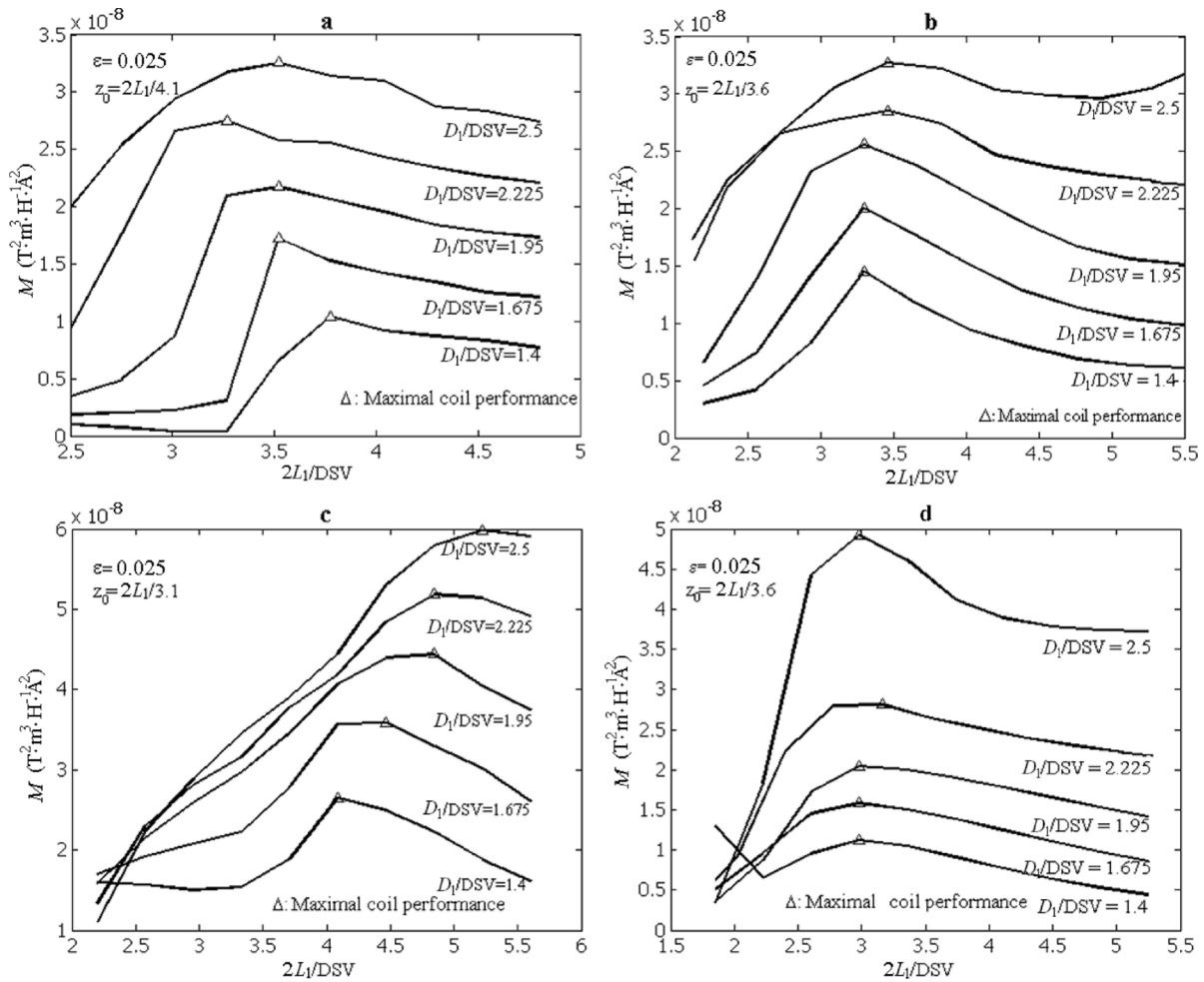


Fig. 2. Four of the several plots of coil performance  $M$  versus normalized coil length  $2L_1/\text{DSV}$ , coil diameter  $D_1/\text{DSV}$ , axial DSV position  $z_0$ , and relaxing factor  $\epsilon$ . a, b, c: Three plots of coil performance  $M$  versus normalized coil length  $2L_1/\text{DSV}$ , coil diameter  $D_1/\text{DSV}$ , axial DSV position  $z_0 = (2L_1/4.1, 2L_1/3.6, 2L_1/3.1)$ ,  $\epsilon = 0.025$ , and  $N = 2$ . d: One case of unshielded asymmetric gradient coil performance assuming  $N = 1$ , for DSV position  $z_0 = 2L_1/3.6$  and a relaxation target uniformity factor  $\epsilon = 0.025$ .

case when  $N = 2$  is studied and the results are extended to any case where  $N \geq 2$ .

Fig. 2 shows some of the cases where the coil performance  $M$  is plotted against the ratio  $2L_1/\text{DSV}$  for fixed  $D_1/\text{DSV}$ , relaxing factor  $\epsilon = 0.025$ , DSV axial position  $z_0 = (2L_1/4.1, 2L_1/3.6, 2L_1/3.1)$ , and  $N = 2$  for asymmetric shielded transverse gradient coils. See Fig. 2(a)–(c). One case for DSV axial position  $z_0 = 2L_1/3.6$ , relaxing factor  $\epsilon = 0.025$ , and number of current layer  $N = 1$  (unshielded) is shown in Fig. 2(d).

Note that in the range of the normalized values of  $2L_1/\text{DSV}$ , an optimal coil length value that generates maximal coil performance is produced.

Coils with relative large DSV ( $\text{DSV} > 0.5\rho_1$ ), DSV axial position close to the coil edge ( $z_0 < 2L_1/4.1$ ), and relaxing factor  $\epsilon < 0.025$  (relative high uniformity) produce unreliable current patterns characterized by poor coil performance. For a fixed  $2L_1/\text{DSV}$ ,  $D_1/\text{DSV}$ ,  $N$  current layers and a relaxing factor  $\epsilon$  when the axial offset position of DSV ( $z_0$ ) approaches from the coil edge to the coil center, the coil performance  $M$  increases, as Fig. 2(a)–(c) illustrates. At the same time, larger axial coil length is required to produce the maximal coil figure of merit

$M$ . If one of the main objectives is to obtain short gradient coils, it is recommended to locate the axial DSV position ( $z_0$ ) close to the coil entrance ( $z_0 = 2L_1/4.1$ ) to produce such solutions. Coils with a DSV axial position very close to the coil entrance ( $z_0 \leq 2L_1/4.1$ ) can be achieved by using a relaxation factor  $\epsilon$  larger than 0.025 (target gradient field of relative low uniformity) while keeping the same coil figure of merit. These curves demonstrate that an arbitrary coil length could produce poor coil performance when a short coil is desired.

The comparison of Fig. 2(b) and (d) indicates that the coil performance for  $N = 1$  (unshielded) is 1.5 times larger than when  $N \geq 2$  (shielded) for the same relaxing factor  $\epsilon$  and DSV axial position  $z_0$  values. At the same time, the unshielded asymmetric gradient coil requires less coil axial length than the shielded case to produce maximal figure of merit  $M$ .

We note that the coil performance  $M$  value increases almost 1.5 times when the relaxing factor  $\epsilon$  value is increased 2 times. It confirms that one of the ways to enhance coil performance is relaxing the target gradient uniformity through the  $\epsilon$  parameter.

For fixed relaxing factor  $\epsilon$  and axial DSV position  $z_0$ , the coordinate ( $D_1/\text{DSV}$ ,  $2L_1/\text{DSV}$ ) where the coil produces maximal figure of merit  $M$  is plotted and fitted based on linear re-

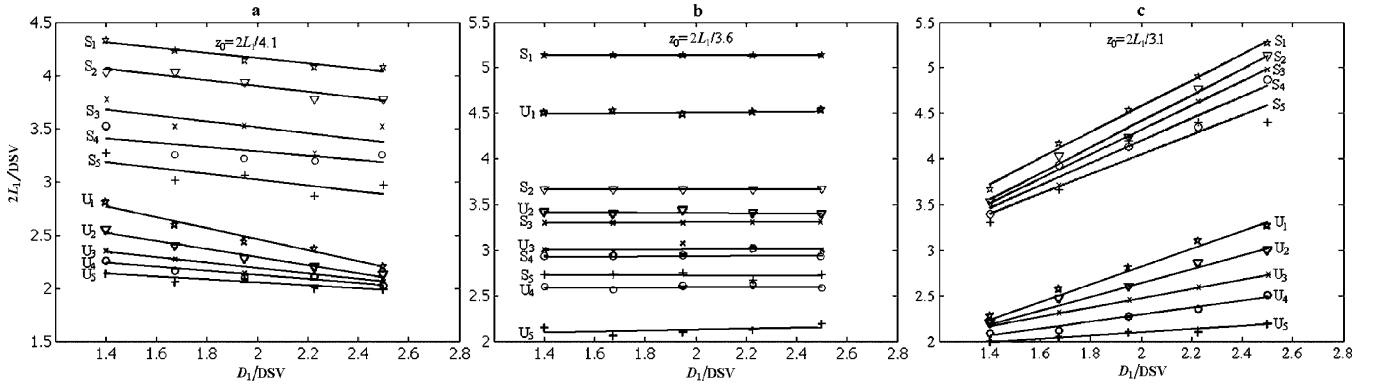


Fig. 3. Linear relationship that defines the optimal coil length to produce maximal figure of merit  $M$  given DSV, coil radius ( $\rho_1$ ), relaxing factor  $\varepsilon$ , and DSV axial position  $z_0$ . U and S means unshielded and shielded case, respectively.

gression producing a relationship for the optimal coil length that generates maximal coil performance  $M$  as function of coil diameter  $D_1$ , DSV, relaxing factor  $\varepsilon$ , and axial DSV position  $z_0$ . Fig. 3(a)–(c) shows the linear functions for the shielded ( $N \geq 2$ ) and unshielded ( $N = 1$ ) asymmetric, transverse gradient coils.

Table I shows the parameters of the linear functions for three different  $z_0$ -positions and five relaxing values of  $\varepsilon$ . Depending on the  $z_0$  value, the linear relationship presents three dependencies with the coil diameter  $D_1$ : negative slope, close to zero, and positive slope. Negative means that for  $z_0 = 2L_1/4.1$ , fixed DSV and relaxing factor  $\varepsilon$  value, the coil length should be reduced when the coil diameter  $D_1$  is increased. Close to zero slope ( $z_0 = 2L_1/3.6$ ) implies that the coil length is determined by the DSV and the relaxing factor  $\varepsilon$ . In other words, the maximal coil performance  $M$  appears in the same axial position when the  $D_1/DSV$  ratio is varied for a fixed relaxing value  $\varepsilon$ . Positive slope indicates that the DSV axial position  $z_0$  is relatively close to the coil center ( $z_0 = 2L_1/3.1$ ) and larger coil axial length is required to fulfill the field constraints in (18). In this situation, reverse turns can appear at the coil entrance ( $\rho_n, \phi, 0$ ) contributing to the minimization of the net torque and peripheral nerve stimulation (PNS) [15].

Although these linear functions have been derived for the optimal axial coil length that produces maximal coil performance  $M$ , it is possible to obtain short gradient coils without significantly reducing the value of figure of merit  $M$  [4] as Fig. 2(a)–(d) demonstrate. However, taking into account the rate of change of the figure of merit  $M$  in respect to the ratio  $2L_1/DSV$  around the maximum performance point, we recommend this approach only for coil diameters larger than the DSV, specifically for the ratio  $D_1/DSV > 1.675$ .

As expected, if a high gradient uniformity is desired then a larger axial coil length is required (see Fig. 3).

In order to provide a comparison to known designs, we consider a transverse asymmetric gradient coil for head imaging [9]. In order to use the linear rule  $S_5$ , we set  $\varepsilon = 0.1$ ,  $\rho_1 = 0.168$  m (head coil),  $\rho_2 = 1.631 \cdot \rho_1$ ,  $DSV = \rho_1$ , and  $z_0 = 2L_1/4.2$ . Applying this rule, we obtain that the optimal coil axial length for the layer  $n = 1$  and  $n = 2$  are  $2L_1 = 50.74$  cm and  $2L_2 = 62.92$  cm ( $2L_2 = 1.24 \cdot 2L_1$ ), respectively. The target points to control the stray field were located at a shielding surface of radius  $\rho_{SS} = 0.5$  m. The resulting figure of merit  $M$  was

TABLE I  
LINEAR FUNCTION PARAMETERS AND RELAXING FACTOR  $\varepsilon$  VALUES FOR (S)HIELDED AND (U)NSHIELDED MULTILAYER ASYMMETRIC TRANSVERSE GRADIENT COILS WITH DIFFERENTS DSV AXIAL POSITIONS  $z_0$ .

Shielded Transverse Gradient Coil									
$z_0 = 2L_1/4.1$	$m$	$b$	$z_0 = 2L_1/3.6$	$m$	$b$	$z_0 = 2L_1/3.1$	$m$	$b$	$\varepsilon$
$S_1$	-0.24	4.65	$S_1$	$-4.7 \times 10^{-3}$	5.14	$S_1$	1.43	1.72	$1 \cdot 10^{-2}$
$S_2$	-0.28	4.45	$S_2$	$4.6 \times 10^{-3}$	3.66	$S_2$	1.43	1.55	$2.58 \cdot 10^{-2}$
$S_3$	-0.28	4.07	$S_3$	$1.8 \times 10^{-2}$	3.27	$S_3$	1.34	1.64	$5.05 \cdot 10^{-2}$
$S_4$	-0.20	3.69	$S_4$	$3.0 \times 10^{-2}$	2.89	$S_4$	1.22	1.75	$7.53 \cdot 10^{-2}$
$S_5$	-0.27	3.56	$S_5$	$-2.0 \times 10^{-2}$	2.77	$S_5$	1.07	1.90	$10 \cdot 10^{-2}$
Unshielded Transverse Gradient Coil									
$z_0 = 2L_1/4.1$	$m$	$b$	$z_0 = 2L_1/3.6$	$m$	$b$	$z_0 = 2L_1/3.1$	$m$	$b$	$\varepsilon$
$U_1$	-0.52	3.49	$U_1$	$1.8 \times 10^{-2}$	4.47	$U_1$	0.92	1.00	$1 \cdot 10^{-2}$
$U_2$	-0.38	3.05	$U_2$	$-1.1 \times 10^{-2}$	3.43	$U_2$	0.72	1.22	$2.58 \cdot 10^{-2}$
$U_3$	-0.25	2.69	$U_3$	$1.9 \times 10^{-2}$	2.97	$U_3$	0.5	1.46	$5.05 \cdot 10^{-2}$
$U_4$	-0.19	2.50	$U_4$	$7.0 \times 10^{-3}$	2.58	$U_4$	0.39	1.51	$7.53 \cdot 10^{-2}$
$U_5$	-0.13	2.31	$U_5$	$-5.0 \times 10^{-2}$	2.02	$U_5$	0.17	1.76	$10 \cdot 10^{-2}$

$$2L_1 = m \cdot D_1 + b \cdot DSV^*$$

\*  $2L_1, D_1$  are the axial coil length and the diameter of the current layer  $n = 1$ . The  $\varepsilon$  value represents the relaxing factor of the target gradient uniformity in the DSV.  $z_0$  is the DSV axial position. S and U represents the five linear relationships for (S)hielded and (U)nsielded transverse gradient coils.

equal to  $3.08 \times 10^{-8} \text{ T}^2 \cdot \text{m}^3 \cdot \text{H}^{-1} \cdot \text{A}^{-2}$ . The gradient nonuniformity within 5% of relative deviation from  $G_0$  is extended 16.4 and 21.8 cm along the axial and transverse axis, respectively. It is important to note the strong tradeoff between coil performance and the generated gradient uniformity. Both characteristics have been improved in the present design in comparison with the [9]. The resulting coil efficiency and inductance was  $\eta = 0.1145 \cdot 10^{-3} \text{ T/m} \cdot \text{A}$  and  $L = 56.97 \mu\text{H}$ , respectively. The measured distance ( $\xi \cdot \rho_1$ ) from the coil edge to the 5% contour of gradient uniformity is equal to 3.9 cm. The parameter  $\xi$  is defined as the distance from the region of 5% of relative gradient uniformity to the coil entrance divided by the coil radius  $\rho_1$  [16]. A small value of  $\xi$  is desired for clinical purposes and patient comfort [16]. Fig. 4(a) shows the integrated current density of the two-layer asymmetric transverse gradient coil.

From the integrated current density and current pattern shown in Fig. 4(a), (b), and (d), we note that the coil winding is not concentrated in a specific region of the cylindrical supporting surface. This kind of current density behavior can simplify the cooling system of the gradient coil. Note in Fig. 4(c), the large region of high gradient uniformity close to the coil entrance.

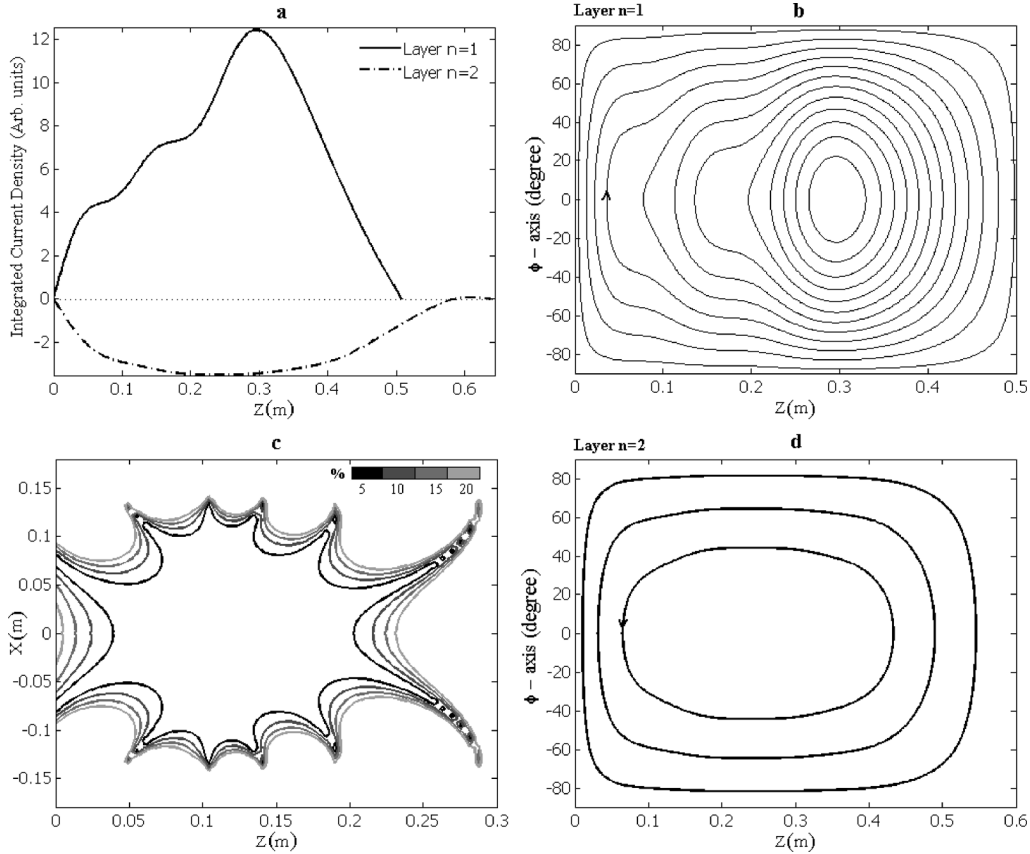


Fig. 4. a: Integrated current density in the two layers asymmetric transverse gradient coils. b and d: the current pattern corresponding to both layers. Note that coil length of the second layer is smaller than the value predicted. This effect is produced when the shielding condition is not stringent. c: Contour plots corresponding to 5%, 10%, 15%, and 20% levels of nonuniformity gradient produced by the discrete asymmetric transverse gradient coil.

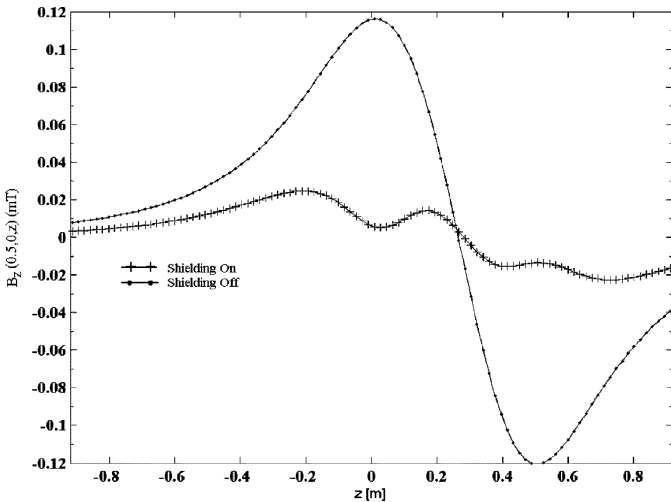


Fig. 5. Axial component of the magnetic field measured along the axial axis at  $\rho_{SS} = 0.5$  m. The solid line represented with + (•) symbols shows the shielded (unshielded) magnetic field. Note that the axial coil domain is extended along the axial axis from  $z = 0$  m to  $z = 0.6292$  m.

In order to evaluate the shielding efficiency of the layer  $n = 2$ , the axial component of the magnetic field was calculated at the shielding surface for two situations. For the first one, the operating current for the layers  $n = 1$  and  $n = 2$  was set to 88 A (shielding on) and for the second one, the current was set to 0

TABLE II  
AMPLITUDES ( $a_{n,q}$ ) OF THE TEN ( $Q = 10$ ) AXIAL OSCILLATION MODES OF THE CURRENT DENSITY THAT DESCRIBES THE ASYMMETRIC TRANSVERSE GRADIENT COIL SHOWN IN FIG. 4. ALL VALUES HAVE BEEN DIVIDED BY A FACTOR OF 1000

$a_{11}$	$a_{12}$	$a_{13}$	$a_{14}$	$a_{15}$	$a_{16}$	$a_{17}$	$a_{18}$	$a_{19}$	$a_{110}$
5.707	-1.326	-0.257	2.901	0.424	-0.498	0.872	1.654	0.942	0.156
$a_{21}$	$a_{22}$	$a_{23}$	$a_{24}$	$a_{25}$	$a_{26}$	$a_{27}$	$a_{28}$	$a_{29}$	$a_{210}$
-1.562	-0.762	-0.215	-0.798	-0.081	-0.440	-0.174	-0.259	-0.094	-0.172

A in the current layer  $n = 2$  (shielding off). The axial component of the magnetic field was evaluated in 100 points over a cylindrical surface of radius  $\rho_{SS} = 0.5$  m and axial length  $L_{SS} = 1.84$  m. Fig. 5 shows the axial component of the magnetic field for both cases. The shielding efficiency measured as the  $\max |B_{z\text{Shielded}}| / \max |B_{z\text{Unshielded}}| \cdot 100$  was equal to approximately 20%.

Table II illustrates the amplitude of the 10 axial modes of the current density that describes the asymmetric transverse gradient coil shown in Fig. 4(b) and (d).

In order to calculate forces and torques, the coil system was placed theoretically in the bore of an ultrashort 1.5 T superconducting magnet [1]. The resulting torque was  $0.753 \text{ N} \cdot \text{m/A}$  and the remaining force  $0.194 \text{ N/A}$ . The second layer acting as shielding reduces the torque up to 20%.

The designs algorithms were run on a PC Pentium 4 CPU, 3 GHz. The CPU time required to calculate the stored magnetic energy (10), force/torque components (11) and (15), mag-

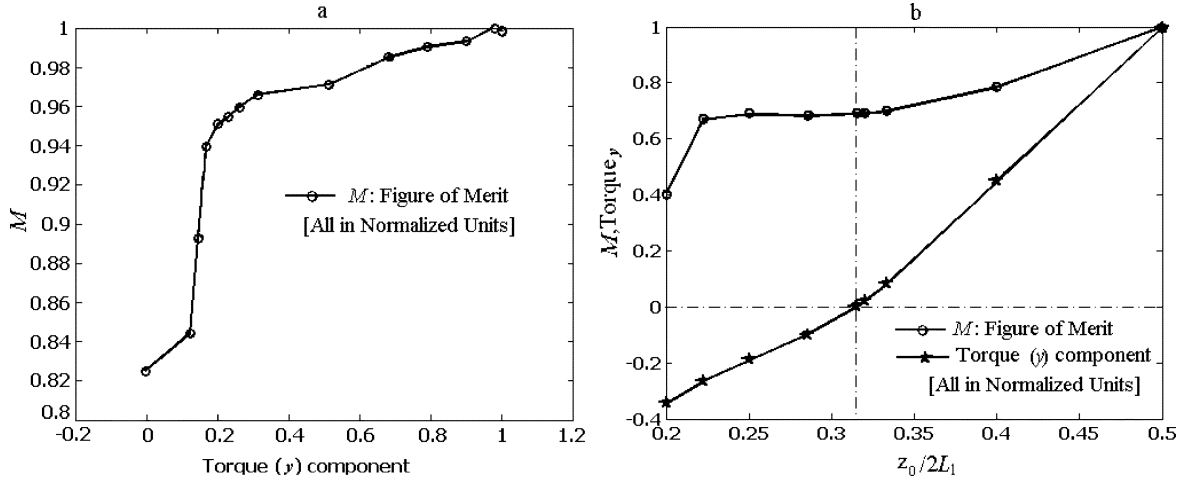


Fig. 6. Target torque minimization and its influence over the coil performance  $M$ . a: Note that a significant reduction in torque value can be achieved without large detriment in figure of merit  $M$ . b: Plot of the DSV relative axial position  $z_0$  versus torque and coil performance. Note that it is possible to obtain a torque balanced asymmetric gradient coil by combining the external magnetic field with a specific axial position of the gradient coil's linear region. All the magnitudes have been normalized.

netic field (3), gradient (5) and to solve the optimization problem stated in (18) was around 5.5 min. The evaluation of the discrete coil in terms of the magnetic gradient field in the DSV, magnetic field at the shielding surface, inductance, force, and torque took approximately 21.5 min, whereby around 70% of that time was spent computing the inductance in the real space.

#### A. A Simple Torque Balancing Approach

Torque is a distinctive and undesired problem in gradient coils; for this reason different strategies to minimize this parameter have been presented [10]–[12]. It is difficult to control the expected minimum torque/force values using these methods and hence the resultant influence over figure of merit  $M$ . In this work, we present two ways to minimize the net torque/force in asymmetric gradient coils. In the first method, we include the target torque constraint in (18) and we study its influence over the coil performance  $M$ . In the second method, the gradient coil is balanced by a combining the external magnetic field ( $\mathbf{B}^{\text{main}}$ ) effect over the gradient coil with a specific axial position  $z_0$  of the gradient coil's linear region. Another possible method to minimize torque is to use more than two current density layers and to locate one of them in certain radius larger than  $\rho_{n=N}$ . This approach is not practical when the radial space within the magnet bore is constrained, and for this reason such implementation has not been presented in this paper.

Applying the first strategy of torque minimization we have studied the torque effect over the figure of merit  $M$  constraining the value of the  $y$  component of torque in the range between 0 to 66.23 N·m for the unbalanced two-layer asymmetric transverse gradient coil shown in Fig. 4(a). To assure maximal coil performance, we have used the linear function  $S_5$  presented in Table I. Applying our target torque minimization technique, we find that if the torque is reduced up to 80% [see Fig. 6(a)], the coil performance  $M$  value decreases by only 5%; however, for torque reduction larger than 80%, the winding complexity increases incrementing the coil inductance and hence reduced values of the figure of merit are attained.

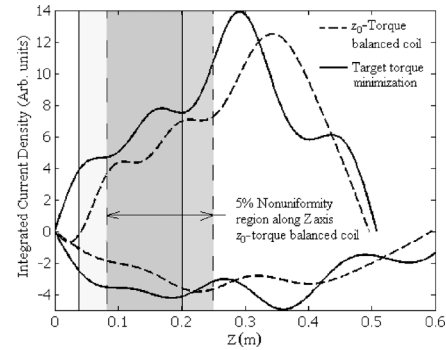


Fig. 7. Integrated current density for the  $z_0$ -torque balanced coil and target torque minimization strategy. The shadow region contained between the dashed lines represents the 5% nonuniformity region produced by the  $z_0$ -torque balanced coil. The shadow region between the continuous lines represents the 5% nonuniformity region produced by the target  $z_0$ -torque balanced coil.

In order to study the influence of the axial DSV position  $z_0$  over the figure of merit and the torque, we have evaluated the example presented in Fig. 4(a) and Table II for different normalized positions of the DSV along the  $z$ -axis. Fig. 6(b) shows the axial DSV position  $z_0$  influences over the torque and coil performance. We note from the plots that it is possible to generate torque balanced gradient coils with zero torque and at the same time to produce high performance gradient coils.

In order to illustrate both methods through a practical situation we have redesigned the asymmetric gradient coil presented in Fig. 4(a), now constraining the  $y$  component of torque between the target values  $-0.5$  N·m and  $0.5$  N·m. From Fig. 6(b), we set  $z_0 = 2L_1/3.125$  to produce a  $z_0$ -torque balanced coil. In both coils the remaining torque was 0.42 N·m.

Fig. 7 shows the integrated current density for both designs. Note that the  $z_0$ -torque balanced coil produces a smoother integrated current than the constrained torque coil. However, the distance  $\xi \cdot \rho_1$  in the  $z_0$ -torque balanced case is 1.85 times larger than the distance  $\xi \cdot \rho_1$  in the target torque constrained case.

Table III shows two torque unbalanced asymmetric transverse gradient coils and four torque balanced designs. Comparing the

TABLE III  
PARAMETERS OF TORQUE UNBALANCED AND BALANCED ASYMMETRIC TRANSVERSE GRADIENT COILS

Author	5% non-uniformity region in XZ plane	$M$ $\times 10^{-8}$ ( $T^2 m^3 H^{-1} A^{-2}$ )	$\xi \cdot \rho_1$ (cm)	Torque (N·m/A/T)
Unbalanced*	16.4 cm x 21.8 cm	3.08	3.90	0.50
Unbalanced [9]	16 cm x 21 cm	2.48	~6	0.54
Target torque minimization*	16.2 cm x 19 cm	2.65	3.83	$3.20 \times 10^{-3}$
$z_0$ -torque balanced*	16.7 cm x 18 cm	3.00	7.09	$3.20 \times 10^{-3}$
Torque balanced [10] (Unshielded)	~15 cm ( $\rho_1=13.6$ cm)	0.73	~9	~0
Torque balanced [11] (Unshielded)	~16 cm ( $\rho_1=16$ cm)	4.70	~9	~0

\*This work.  $M$  represents the figure of merit and  $(\xi \cdot \rho_1)$  is the distance from the coil edge to the 5% contour of the gradient uniformity map.

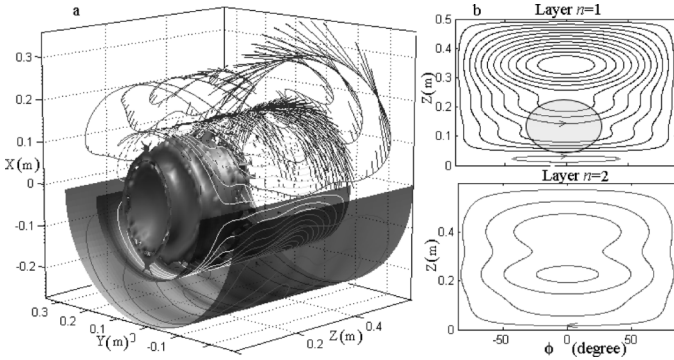


Fig. 8. Three-dimensional current pattern representation of the  $z_0$ -torque balanced gradient coil. a: In the top half of the coil, the torque vector produced at each wire segment is illustrated. a: The surface represented in the bottom coil half shows in grayscale the pressure produced by the winding over the coil support. a: The 5% nonuniformity gradient isosurface is also illustrated. b: One half current pattern of the asymmetric  $z_0$ -torque balanced transverse gradient coil. The shadowed circle represents the gradient uniformity region (DSV).

design presented in this work, we note that a reduction of coil performance is obtained when torque minimization is included in the optimization problem (18).

Comparing the torque balanced approach [10] and [11] with the constrained torque and  $z_0$ -torque balanced asymmetric transverse gradient coils presented in this work, it is evident that our design methodology has produced a gradient uniformity region that is larger than those in the referenced works [10], [11]. Moreover, the DSV position in our designs is closer to the coil entrance (small  $\xi \cdot \rho_1$ ). In addition, the torque value is not zero in order to keep a high coil performance value. A relatively high coil performance is produced by the design [11] due to the reversal turns close to the coil entrance and the lack of a shielding coil.

Fig. 8(a) shows the three-dimensional current pattern of the  $z_0$ -torque balanced coil system. The schematic representation of the torque acting over each segment of wire shown in Fig. 8(a) indicates which part of the coil could suffer more mechanical fatigue and the region of the coil where the winding acts with more pressure over the coil support.

The maximal pressure produced by the winding over surface support  $n = 1$  at the axial position ( $\rho_1 = 0.168$  m,  $\phi = 0$ ,  $z = 0.49$  m) is 175.6901 Pa/A and in the surface  $n = 2$  is 62.7608 Pa/A in the position ( $\rho_2 = 0.2740$  m,  $\phi = 0$ ,  $z = 0.245$  m), respectively.

Fig. 8(b) illustrates a reverse turn at the coil entrance in the layer  $n = 1$  that creates torque balance and can possibly reduce PNS [15] as described in Section III-B.

The presented methodology can be extended to planar gradient coil design [17].

### B. Peripheral Nerve Stimulation Reduction

The switching of magnetic field gradients in MRI induces transient electric fields in the patient, which may cause peripheral nerve stimulation (PNS). PNS ultimately limits the gradient performance in terms of the field strength, gradient rise time, and switching frequency [18].

One of the main goals of this study was to balance the torque on the coil, which was achieved by target torque minimization and  $z_0$ -torque balance method. As a consequence of the last approach, reverse turns are generated at the coil entrance. This type of solution serendipitously also reduces the electric field and consequently PNS within the patient [15].

In order to evaluate how much of the induced electric field can be reduced within the patient, we have computed the total electric field inside an inhomogeneous head model of the **Normalized Man** voxel phantom (NORMAN) [19] induced by the  $z_0$ -torque balanced coil and compared the simulation results to those of the unbalanced asymmetric gradient coil. The conductivity values of all head-identified tissue types were frequency scaled and kept constant at 1 kHz. At such low frequencies, vector magnetic potential is the dominant component of the total electric field and can be computed with Biot–Savart’s law without the consideration of the human head. However, for an accurate assessment of the electric field in the tissue, the secondary field should be also taken into account. The scalar electric potential is obtained with the previously developed in-house quasi-static finite-difference scheme by assuming sinusoidal current excitation in the gradient coils [20]. Fig. 9 demonstrates a three-dimensional representation of induced total electric field in the human head due to the unbalanced and  $z_0$ -torque balanced, asymmetric,  $x$ -gradient head coil.

The comparison of the electric field profiles induced by Unbalanced ( $E_U$ ) and Balanced coils ( $E_B$ ) shows that more electric field is induced in the head by the unbalanced than by the torque balanced coil. As expected, the regions with large magnetic field gradients imply high electric field in the tissue particularly near

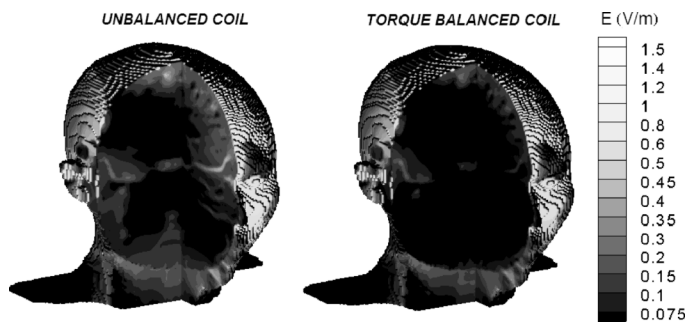


Fig. 9. Three-dimensional representation of the induced total electric field in the human head due to the unbalanced ( $E_U$ ) and  $z_0$ -torque balanced ( $E_B$ ) asymmetric transverse gradient coil for head imaging.

the coil ends. The presence of the negative turns at the coil entrance of the torque-balanced coil mitigates the spatial magnetic field change near the DSV periphery.

#### IV. CONCLUSION

In this work, we have studied the relationship between the target field uniformity, coil dimensions, and the figure of merit  $M$  for asymmetric, multilayer, transverse gradient coils. A simple linear function that defines the optimal coil length to maximize the figure of merit given other fixed parameters has been derived. Applying the method and the linear functions described in this work, solutions with superior figure of merit–gradient uniformity tradeoff are obtained. The benefit of using the target nonuniformity error rather than the conventional weighting factor is that one has more control over the coil performance and hence the ability to balance gradient uniformity and figure of merit requirements.

A method for producing asymmetric transverse gradient coils with minimum torque and relatively high performance has been presented. A reduction of up to 80% in net torque only decreases the figure of merit by 5% from its maximum value. Torque reduction larger than 80% can produce solutions with poor coil performance.

We have illustrated that by combining the external magnetic field profile with a certain axial position of the gradient coil's linear region, it is possible to produce head asymmetric gradient coils with a minimum net torque. We have shown solutions where negative turns are generated at the coil entrance and that this structure can also potentially reduce PNS in the human head.

#### ACKNOWLEDGMENT

This work was supported by the Australian Research Council. The authors would like to thank Dr. P. J. Dimbylow (NRPB, UK) for providing the NORMAN model.

#### REFERENCES

- [1] S. Crozier, H. Zhao, and D. M. Doddrell, "Current density mapping approach for design of clinical magnetic resonance imaging magnets," *Concepts Magn. Reson.*, vol. 15, pp. 208–215, 2002.
- [2] G. DeMeester, M. Morich, A. Byrne, F. Davies, D. Melotte, and A. Thomas, "Challenges of short magnet design," *Magma*, vol. 13, pp. 193–198, 2002.
- [3] H. Xu, S. Conolly, G. C. Scott, and A. Macovski, "Fundamental scaling relations for homogeneous magnets," in *Proc. 7th Annu. Meeting ISMRM*, Philadelphia, PA, 1999, p. 475.
- [4] B. Zhang, C. Gazdzinski, B. A. Chronik, H. Xu, S. M. Conolly, and B. K. Rutt, "Simple design guidelines for short MRI systems," *Concepts Magn. Reson.*, vol. 25B, pp. 53–59, 2005.
- [5] J. W. Carlson, K. A. Derby, K. C. Haveryszko, and M. Weideman, "Design and evaluation of shielded gradient coils," *Magn. Reson. Med.*, vol. 26, pp. 191–206, 1992.
- [6] J. Leggett, S. Crozier, S. Blackband, B. Beck, and R. Bowtell, "Multilayer transverse gradient coil design," *Concepts Magn. Reson.*, vol. B16, pp. 38–46, 2003.
- [7] R. A. Lemdiasov and R. A. Ludwig, "Stream function method for gradient coil design," *Concepts Magn. Reson.*, vol. 26B, pp. 67–80, 2005.
- [8] B. L. W. Chapman and P. Mansfield, "A quiet gradient-coil set employing optimized, force-shielded distributed coil designs," *J. Magn. Reson.*, vol. B107, pp. 152–157, 1995.
- [9] D. Tomasi, R. F. Xavier, B. Foerster, H. Panepucci, A. Tannús, and E. L. Vidoto, "Asymmetrical gradient coil for head imaging," *Magn. Reson. Med.*, vol. 48, pp. 707–714, 2002.
- [10] A. M. Abduljalil, A. H. Aletras, and P.-M. L. Robitaille, "Torque free asymmetric gradient coils for echo planar imaging," *Magn. Reson. Med.*, vol. 31, pp. 450–453, 1994.
- [11] D. C. Alsop and T. J. Connick, "Optimization of torque-balanced asymmetric head gradient coils," *Magn. Reson. Med.*, vol. 35, pp. 875–886, 1996.
- [12] S. Crozier, K. Luescher, G. Hinds, W. U. Roffmann, and D. M. Doddrell, "Designs for an asymmetric gradient set and a compact superconducting magnet for neural magnetic resonance imaging," *Rev. Sci. Instrum.*, vol. 70, pp. 4062–4066, 1999.
- [13] M. Rausch, M. Gebhardt, M. Kaltenbacher, and H. Landes, "Computer-aided design of clinical magnetic resonance imaging scanners by coupled magnetomechanical-acoustic modeling," *IEEE Trans. Magn.*, vol. 41, no. 1, pp. 72–81, Jan. 2005.
- [14] S. H. Shvartsman, M. Morich, G. DeMeester, and Z. Zhai, "Ultrashort shielded gradient coil design with 3D geometry," *Concepts Magn. Reson.*, vol. 26B, pp. 1–15, 2005.
- [15] S. H. Shvartsman, G. DeMeester, and M. Morich, "MRI transverse gradient coil for reduced peripheral nerve stimulation," in *Proc. 13th Annu. Meeting ISMRM*, Miami, FL, 2005, p. 858.
- [16] B. A. Chronik, A. Alejski, and B. K. Rutt, "Design and fabrication of a three-axis edge ROU head and neck gradient coil," *Magn. Reson. Med.*, vol. 44, pp. 955–963, 2000.
- [17] L. K. Forbes, M. A. Brideson, and S. Crozier, "A target-field method to design circular biplanar coils for asymmetric shim and gradient fields," *IEEE Trans. Magn.*, vol. 41, no. 6, pp. 2134–2144, Jun. 2005.
- [18] S. C. Faber, A. Hoffman, C. Ruedig, and M. Reiser, "MRI-induced stimulation of peripheral nerves: Dependency of stimulation threshold on patient positioning," *J. Magn. Reson. Imag.*, vol. 21, pp. 715–724, 2003.
- [19] P. J. Dimbylow, "Current densities in a 2 mm resolution anatomically realistic model of the body induced by low frequency electric fields," *Phys. Med. Biol.*, vol. 45, pp. 1013–1022, 2000.
- [20] F. Liu, H. Zhao, and S. Crozier, "On the induced electric field gradients in the human body for magnetic stimulation by gradient coils in MRI," *IEEE Trans. Biomed. Eng.*, vol. 50, pp. 804–815, 2003.